Effect of Aspect Ratio on the Formation and Surfactant Resistance of Pickering Emulsions Prepared Using Anisotropic Cross-Linked Diblock Copolymer Nanoparticles

Saul J. Hunter,[†] Kate L. Thompson,*[,‡] Joseph R. Lovett,[†] Fiona L. Hatton,[†] Matthew J. Derry,[†] Christopher Lindsay,[$] Philip Taylor[$] and Steven P. Armes*[,†]

[†]Department of Chemistry, Dainton Building, University of Sheffield, Brook Hill, Sheffield, Yorkshire S3 7HF, UK.

[‡] The School of Materials, University of Manchester, Oxford Road, Manchester M13 9PL, UK.

[$] Syngenta, Jealott's Hill International Research Centre, Bracknell, Berkshire, RG42 6EY, UK.

* Authors to whom correspondence should be addressed (s.p.armes@sheffield.ac.uk or kate.thompson@manchester.ac.uk)

ABSTRACT. Reversible addition-fragmentation chain transfer (RAFT)-mediated polymerization-induced self-assembly (PISA) is used to prepare epoxy-functional $PGMA_{48}$-P($HPMA_{90}$-*stat*-$GlyMA_{15}$) diblock copolymer worms, where GMA, HPMA and GlyMA denote glycerol monomethacrylate, 2-hydroxypropyl methacrylate and glycidyl methacrylate, respectively and the subscripts indicate the mean degrees of polymerization. The epoxy groups on the GlyMA residues were ring-opened using 2-aminopropyltriethoxysilane (APTES) in order to cross-link the worm cores *via* a series of hydrolysis-condensation reactions. Importantly, the worm aspect ratio can be adjusted depending on the precise conditions selected for covalent stabilization. Relatively long cross-linked worms are obtained via APTES crosslinking conducted at 20 °C, whereas much shorter worms with *essentially the same copolymer composition* are formed by cooling the linear worms from 20 °C to 4 °C prior to APTES addition. Small-angle X-ray scattering (SAXS) studies confirmed that the mean aspect ratio for the long worms is approximately eight times greater than that for the short worms. Aqueous electrophoresis studies indicated that both types of cross-linked worms acquired weakly cationic surface charge at low pH as a result of protonation of APTES-derived secondary amine groups within the nanoparticle cores. These cross-linked worms were evaluated as emulsifiers for the stabilization of *n*-dodecane-in-water emulsions *via* high-shear homogenization at 20 °C and pH 8. Increasing the copolymer concentration led to a reduction in mean droplet diameter, indicating that APTES cross-linking was sufficient to allow the nanoparticles to adsorb intact at the oil/water interface and hence produce genuine Pickering emulsions, rather than undergo *in situ* dissociation to form surface-active diblock copolymer chains. In surfactant challenge studies, the relatively long worms required a thirty-fold higher concentration of a non-ionic surfactant (Tween 80) to be displaced from the *n*-dodecane-water interface compared to the short worms. This suggests that the former nanoparticles are much more strongly adsorbed than the latter. In contrast, colloidosomes prepared by reacting the hydroxyl-functional adsorbed worms with an oil-soluble polymeric diisocyanate remained intact when exposed to high concentrations of Tween 80.

INTRODUCTION

Pickering emulsions comprise either oil or water droplets stabilized by solid particles and were independently recognized by Pickering[1] and Ramsden[2] over a century ago. Adsorption of particles at the oil/water interface reduces the interfacial area between the two immiscible phases and provides a steric barrier towards droplet coalescence. Whether a water-in-oil (w/o) or oil-in-water (o/w) emulsion is formed depends on the particle wettability at the oil/water interface.[3] Hydrophobic particles are preferentially wetted by the oil phase and so form w/o emulsions. In contrast, hydrophilic particles are preferentially wetted by the aqueous phase and hence favor the formation of o/w emulsions.[4-9] As well as dictating the emulsion type, particle wettability also determines the energy of interfacial detachment through the three-phase contact angle (θ_w).[3] This energy of detachment also depends on the particle radius.[3] For sufficiently large particles, the energy of detachment substantially exceeds their thermal energy, hence they can be considered to be irreversibly adsorbed at the oil/water interface.[3]

Depending on the specific application, demulsification on demand may be desirable. The stability of stimulus-responsive Pickering emulsions can be controlled by varying external stimuli such as temperature,[10-16] pH,[17-24], added salt,[25-27] light,[28-30] or magnetic fields.[31-33] It is also well-known that addition of surfactants to Pickering emulsions can lead to displacement of the adsorbed particles from the oil/water interface if the resulting surfactant-stabilized droplets have a lower free energy than the particle-stabilized droplets.[34-36] There are two mechanisms by which surfactants can displace adsorbed particles: (i) adsorption onto the particle surface, thus altering its wettability and θ_w and leading to particle desorption from the oil/water interface[34] and (ii) competitive surfactant adsorption at the oil/water interface, which lowers the interfacial tension (γ_{ow}) of the emulsion.[35]

The vast majority of Pickering emulsifiers reported in the literature are spherical particles.[4, 5, 37-39] However, considerable recent attention has been directed towards the use of anisotropic particles.[39-50] For example, rigid rods have been evaluated by Vermant and co-workers, who utilized a mechanical

alignment technique to prepare ellipsoidal polystyrene particles with length/width aspect ratios of approximately five.[44, 51] The enhanced stability of Pickering emulsions prepared using such anisotropic latexes relative to their spherical precursor particles was demonstrated using a multiple backscattering technique. Similarly, highly anisotropic cellulosic fibers derived from bacteria have also been explored as emulsifiers for the stabilization of both oil-in-water and water-in-oil emulsions.[52,53-55] For such Pickering emulsions, the droplet surface coverage is strongly dependent on the fiber aspect ratio.[56] A densely-packed layer was formed at the oil/water interface (> 80% surface coverage) when using relatively short fibers, whereas employing longer fibers led to the formation of a more open 2D network (surface coverage ~ 40%).

Recently, we have examined the interfacial activity of flexible diblock copolymer worms of varying surface chemistries prepared *via* polymerization-induced self-assembly (PISA).[57, 58] Such syntheses can be conducted in either *n*-alkanes or water to afford either hydrophobic[59, 60] or hydrophilic[61, 62] diblock copolymer nanoparticles, respectively. For example, *hydrophilic* poly(glycerol monomethacrylate)-poly(2-hydroxypropyl methacrylate) [PGMA-PHPMA] worms and spheres were prepared in water, but these *linear* nanoparticles did not survive the high-energy homogenization conditions required to generate the oil droplets.[57] Stable emulsions were formed, but they were stabilized by individual copolymer chains acting as a soluble polymeric surfactant. Such *in situ* dissociation of the nanoparticles is attributed to the weakly hydrophobic nature of the core-forming PHPMA block.[61, 63] In view of this nanoparticle instability problem, a small amount of ethylene glycol dimethacrylate was added as a third comonomer to form *cross-linked* nanoparticles, which proved to be stable when subjected to high-shear homogenization.[57] Such covalent stabilization allowed the preparation of robust worms and spheres but in this case differing copolymer compositions were required to prepare these two morphologies.

Of particular relevance to the present study, the Pickering emulsifier performance of linear *hydrophobic* poly(lauryl methacrylate)-poly(benzyl methacrylate) [PLMA-PBzMA] worms and spheres were directly

compared by Thompson and co-workers.[58] PLMA-PBzMA worms can be transformed into spheres when heated to 150 °C.[60] Moreover, this morphological transition is effectively irreversible if it is conducted at sufficiently high dilution (e.g. 1.0% w/w copolymer).[58, 60] Thus, the Pickering performance of *hydrophobic* anisotropic worms for the stabilization of w/o emulsions could be compared to that of *chemically identical* spheres for the first time. This is important, because the surface wettability of such nanoparticles is primarily determined by their chemical composition. Adsorption of block copolymer worms at the oil/water interface was estimated to be at least an order of magnitude greater than that of the precursor spheres, with the former nanoparticles retaining a relatively high specific surface area.[58] In the present study, the analogous *hydrophilic* epoxy-functional diblock copolymer worms are prepared *via* reversible addition-fragmentation chain transfer (RAFT) aqueous dispersion copolymerization of HPMA with glycidyl methacrylate (GlyMA), as outlined in Figure 1.

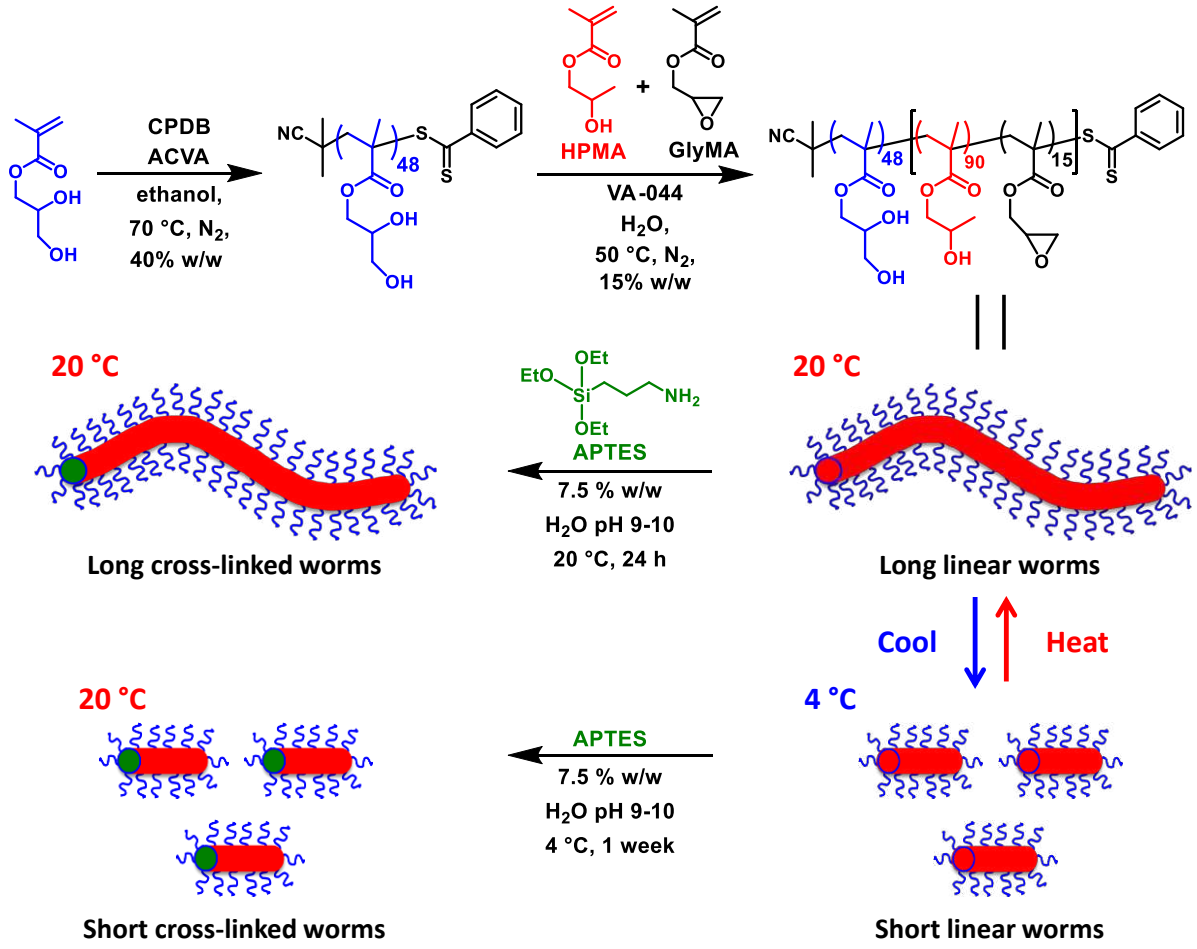

Figure 1. Synthesis of a $PGMA_{48}$ chain transfer agent (CTA) *via* RAFT ethanolic solution polymerization of glycerol monomethacrylate (GMA) using a 2-cyano-2-propyl benzodithioate (CPDB) RAFT agent, and its subsequent chain extension *via* RAFT aqueous dispersion copolymerization of 2-hydroxypropyl methacrylate (HPMA) with glycidyl methacrylate (GlyMA) to form $PGMA_{48}$-P($HPMA_{90}$-*stat*-$GlyMA_{15}$) diblock copolymer worms at 50 °C. Two types of cross-linked $PGMA_{48}$-P($HPMA_{90}$-*stat*-$GlyMA_{15}$) worms that exhibit a relatively high or a relatively low mean aspect ratio can be prepared by post-polymerization reaction with a 3-aminopropylsiloxane (APTES) cross-linker at either 20 °C or 4 °C, respectively. Importantly, such anisotropic nanoparticles have essentially the same copolymer composition.

The thermoresponsive behavior of such linear precursor nanoparticles is exploited to produce either relatively long worms or relatively short worms with essentially the same copolymer composition. More specifically, 3-aminopropyltriethoxysilane (APTES) is utilized in a post-polymerization cross-linking protocol, thereby extending recent work by Lovett *et al.*[64] Small-angle X-ray scattering (SAXS) is used to characterize the mean aspect ratio of these two types of worms. In principle, the highly anisotropic nature of the long worms should lead to a significantly higher energy of detachment compared to the equivalent short worms, as previously discussed by Thompson and co-workers.[58] This hypothesis is evaluated via surfactant challenge studies performed on o/w Pickering emulsions using a non-ionic surfactant (Tween 80).

EXPERIMENTAL

Materials. All reagents were used as received unless otherwise stated. Glycerol monomethacrylate (GMA; 99.8% purity) was kindly donated by GEO Specialty Chemicals (Hythe, UK) and used without further purification. 2-Hydroxypropyl methacrylate (HPMA) was purchased from Alfa Aesar (UK) and used as received. 2,2′-Azobis[2-(2-imidazolin-2-yl)propane] dihydrochloride (VA-044) was purchased from Wako Pure Chemical Industries (Japan) and used as received. Glycidyl methacrylate (GlyMA), 2-cyano-2-propyl benzodithioate (CPDB), 4,4′-azobis(4-cyanopentanoic acid) (ACVA; V-501; 99%), 3-aminopropyltriethoxysilane (APTES), Tween 80, ethanol (99%, anhydrous grade), methanol, dichloromethane, Nile Red, rhodamine B and tolylene 2,4-diisocyanate-terminated poly(propylene glycol) were purchased from Sigma-Aldrich UK. All solvents were of HPLC-grade quality and deionized water was used in all experiments involving aqueous solutions.

Synthesis of Poly(glycerol monomethacrylate) ($PGMA_{48}$) *via* RAFT Solution Polymerization in Ethanol. A round-bottomed flask was charged with GMA (50.0 g, 0.312 mol), CPDB (1.21 g, 5.0 mmol; target DP = 60), ACVA (0.306 g, 1.09 mmol; CPDB/ACVA molar ratio = 5.0), and anhydrous ethanol (77.3 g, 1.67 mol) to afford a 40% w/w solution. The resulting pink solution was purged with N_2 for 25 min before the sealed flask was immersed into an oil bath set at 70 °C. After 150 min (80 % conversion as judged by ^{1}H NMR spectroscopy) the polymerization was quenched by immersion of the flask into an ice bath and subsequently exposing the reaction mixture to air. The crude polymer was then precipitated twice into excess dichloromethane and washed three times with this solvent before being freeze-dried overnight. GPC studies indicated an M_n of 13 000 g mol^{-1} and an M_w/M_n of 1.21.

Synthesis of Linear $PGMA_{48}$−P($HPMA_{90}$-*stat*-$GlyMA_{15}$) Diblock Copolymer Worms *via* PISA. $PGMA_{48}$ macro-CTA (1.20 g, 0.016 mmol), HPMA monomer (2.10 g, 15 mmol), GlyMA monomer (0.344 g, 2.4 mmol; overall target DP = 105), and VA-044 initiator (13.1 mg, 0.04 mmol; $PGMA_{48}$ macro-CTA/VA-044 molar ratio = 4.0) and deionized water (21.0 g, 15% w/w solids) were added to a 50 mL round-bottomed flask. This reaction solution was purged under nitrogen for 30 min at 20 °C prior to immersion into an oil bath set at 50 °C. The copolymerization was quenched by exposure to air after 105 min, followed by cooling to ambient temperature. The resulting dispersion was immediately diluted to 7.5% w/w solids using deionized water.

Synthesis of Fluorescently-Labeled Linear $PGMA_{48}$−P($HPMA_{90}$-*stat*-$GlyMA_{15}$) Diblock Copolymer Long and Short Worms. Rhodamine B piperazine was synthesized as reported elsewhere.[65] Rhodamine B piperazine (22 mg, 0.04 mmol; dye/chain molar ratio = 0.25) was accurately weighed and added to an aqueous copolymer dispersion of long worms (at 20 °C) or short worms (at 4 °C). Each reaction mixture was stirred overnight at either 20 °C or 4 °C. After 20 h, the fluorescently-labeled long worm gel and short worm dispersion was dialyzed against water for one week (with daily changes of dialysate) so as to remove any unreacted dye.

Post-Polymerization Cross-Linking of $PGMA_{48}$−P($HPMA_{90}$-*stat*-$GlyMA_{15}$) Diblock Copolymer Worms Using APTES. APTES (0.27 g, 1.20 mmol, APTES/GlyMA molar ratio = 1.0) was added to 12.0 g of a 7.5% w/w aqueous dispersion of $PGMA_{48}$−P($HPMA_{90}$-*stat*-$GlyMA_{15}$) worms, and the epoxy-amine reaction was allowed to proceed for 16 h at 20 °C with continuous stirring of this shear-thinning dispersion to produce relatively long cross-linked worms. A second batch of the same $PGMA_{48}$−P($HPMA_{90}$-*stat*-$GlyMA_{15}$) diblock copolymer worms was cooled to 4 °C for 2 h to yield a free-flowing dispersion of relatively short worms prior to APTES addition (0.27 g, 1.20 mmol, APTES/GlyMA molar ratio = 1.0). In this case the epoxy-amine reaction was allowed to proceed for one week at 4 °C. Fluorescently-labeled $PGMA_{48}$−P($HPMA_{90}$-*stat*-$GlyMA_{15}$) diblock copolymer long and short worms were cross-linked using the same protocol.

Preparation of Emulsions. *n*-Dodecane (2.0 ml) was homogenized in turn with 2.0 ml of an aqueous dispersion (0.06–2.0% w/w) of either linear or cross-linked long worms (or short worms) for 2 min at 20 °C using a IKA Ultra-Turrax T-18 homogenizer equipped with a 10 mm dispersing tool operating at 13 500 rpm. After appropriate dilution, the resulting oil droplets were imaged by optical microscopy and the mean droplet diameter was determined by laser diffraction.

Colloidosome Formation. PPG-TDI (20.0 g dm^{-3}) was weighed into a sample vial and then dissolved in *n*-dodecane (2.0 ml) prior to homogenization with 2.0 ml of a 0.25% w/w aqueous dispersion of either long or short worms at pH 3 for 2 min at 0 °C using a IKA Ultra-Turrax T-18 homogenizer equipped with a 10 mm dispersing tool operating at 13 500 rpm. The resulting stable milky-white emulsion was allowed to stand at 20 °C for several hours to allow the urethane cross-linking reaction to proceed.

^1H NMR Spectroscopy. All NMR spectra were recorded using a 400 MHz Bruker Avance-400 spectrometer (64 scans averaged per spectrum).

Gel Permeation Chromatography (GPC). 0.50% w/w copolymer solutions were prepared in HPLC-grade DMF containing 10 mM LiBr and DMSO (1.0 % v/v) was used as a flow-rate marker. GPC studies

were conducted at 60 °C using a flow rate of 1.0 mL min^{-1}. The GPC set-up comprised an Agilent 1260 Infinity series degasser and pump, an Agilent PL-gel guard column, two Agilent PL-gel 5 μm Mixed-C columns and a refractive index detector. Sixteen near-monodisperse poly(methyl methacrylate) standards ranging from M_p = 645 to 2 480 000 g mol^{-1} were used for calibration.

Dynamic Light Scattering (DLS). Studies were conducted at 25 °C on 0.10% w/w copolymer dispersions in either water, methanol, or a 1.0% w/w aqueous surfactant solution before and after APTES cross-linking using a Malvern Zetasizer NanoZS instrument equipped with a glass cuvette. Light scattering was detected at a fixed angle of 173°. Intensity-average hydrodynamic diameters were calculated *via* the Stokes−Einstein equation using a non-negative least-squares (NNLS) algorithm. All data were averaged over three consecutive runs.

Aqueous Electrophoresis. Studies were performed on 0.10% w/w aqueous copolymer dispersions (containing 1 mM KCl as background electrolyte) at 25 °C a Malvern Zetasizer NanoZS instrument. The copolymer dispersion pH was initially basic and adjusted as required using HCl. Zeta potentials were calculated from the Henry equation using the Smoluchowski approximation. All data were averaged over three consecutive runs.

Transmission Electron Microscopy (TEM). As-prepared copolymer dispersions were diluted 150-fold at 20 °C in either methanol or water to generate 0.10% w/w dispersions. Copper/palladium TEM grids (Agar Scientific, UK) were surface-coated in-house to yield a thin film of amorphous carbon. The grids were then plasma glow-discharged for 30 s to create a hydrophilic surface. A micropipet was used to place droplets (12 μL) of aqueous copolymer dispersions onto freshly glow-discharged grids for 1 min, followed by careful blotting with filter paper to remove excess sample. To stain the aggregates, a 0.75% w/w uranyl formate solution (9 μL) was soaked on the sample-loaded grid for 20 s and then carefully blotted to remove excess stain. Each grid was then carefully dried using a vacuum hose. Imaging was performed using a FEI Tecnai Spirit microscope fitted with a Gatan 1kMS600CW CCD camera operating at 80 kV.

Optical Microscopy (OM). Optical microscopy images were recorded using a Motic DMBA300 digital biological microscope equipped with a built-in camera and Motic Images Plus 2.0 ML software.

Fluorescence Microscopy. Fluorescence microscopy images of the o/w precursor emulsions were recorded on a Zeiss Axio Scope A1 microscope fitted with the AxioCam 1Cm1 monochrome camera. Nile Red was dissolved in the *n*-dodecane phase prior to emulsification. Nile Red-stained oil droplets and rhodamine-labeled nanoparticles were imaged using Zeiss filter set 43 HE (excitation wavelength = 550/25 nm and emission wavelength = 605/70 nm). Images were captured and processed using ZEN lite 2012 software.

*Laser Diffraction***.** Each emulsion was sized by laser diffraction using a Malvern Mastersizer 3000 instrument equipped with a hydro EV wet sample dispersion unit, a red HeNe laser operating at 633 nm and a LED blue light source operating at 470 nm. The stirring rate was adjusted to 1500 rpm in order to avoid creaming of the emulsion droplets during analysis. After each measurement, the cell was rinsed once with ethanol and three times with deionized water and the laser was aligned centrally to the detector prior to data acquisition.

Small-angle X-ray scattering. SAXS patterns were collected at a synchrotron source (ESRF, station ID02, Grenoble, France) using monochromatic X-ray radiation (wavelength λ = 0.0995 nm, with q ranging from 0.015 to 1.5 nm^{-1} and 0.002 to 0.2 nm^{-1}, where $q = 4\pi \sin\theta/\lambda$ is the length of the scattering vector and θ is one-half of the scattering angle) and a Ravonix MX-170HS CCD detector. Glass capillaries of 2 mm diameter were used as a sample holder and the sample temperature was controlled using a HFSX350-CAP heating/cooling capillary holding stage (Linkam Scientific Instruments Ltd., Tadworth, UK), with 2 min allowed for thermal equilibration prior to data collection. Scattering data were reduced using standard routines from the beamline and were further analyzed using Irena SAS macros for Igor Pro.[66] Water was used for the absolute intensity calibration. Measurements were conducted on 1.0% w/w aqueous dispersions of cross-linked $PGMA_{48}$-P($HPMA_{90}$-*stat*-$GlyMA_{15}$) worms.

RESULTS AND DISCUSSION

Synthesis of cross-linked PGMA$_{48}$-P(HPMA$_{90}$-*stat*-GlyMA$_{15}$) worms. A well-defined near-monodisperse PGMA macro-CTA was prepared *via* RAFT solution polymerization of GMA in ethanol at 70 °C using CPDB as the RAFT agent (see Figure 1). Following purification, a mean DP of 48 was indicated by end-group analysis using ^{1}H NMR spectroscopy (see Figure S1). Gel permeation chromatography (GPC) studies conducted in DMF using a series of near-monodisperse poly(methyl methacrylate) (PMMA) calibration standards indicated that this PGMA$_{48}$ macro-CTA possessed a narrow molecular weight distribution (MWD) (M_n = 13 000 g mol^{-1} and M_w/M_n = 1.21, see Figure S3).

Linear PGMA$_{48}$-P(HPMA$_{90}$-*stat*-GlyMA$_{15}$) diblock copolymer nanoparticles were prepared by chain extension of the PGMA$_{48}$ macro-CTA *via* statistical copolymerization of a mixture of HPMA and GlyMA at 15% w/w solids in aqueous solution at 50 °C (see Figure 1). The target degree of polymerization (DP) of the core-forming block and its GlyMA content were carefully selected so that the resulting diblock copolymer chains self-assembled *in situ* to form a highly anisotropic worm-like morphology during PISA. ^{1}H NMR spectroscopy studies indicated that an overall comonomer conversion of more than 99% was achieved, as judged by the disappearance of the methacrylic vinyl signals between 5.6 and 6.2 ppm (see Figure S2). DMF GPC analysis of this diblock copolymer indicated an M_n of 30 000 g mol^{-1}.

Furthermore, comparison of this GPC curve to that obtained for the PGMA$_{48}$ macro-CTA precursor indicated that a high blocking efficiency was achieved. However, a weak high molecular weight shoulder was observed for PGMA$_{48}$-P(HPMA$_{90}$-*stat*-GlyMA$_{15}$). This is most likely the result of light branching arising from dimethacrylate impurities in the HPMA monomer and/or a side-reaction between HPMA and GlyMA.[67, 68] ^{1}H NMR analysis of this diblock copolymer suggests that minimal hydrolysis of the pendent epoxy groups occurs during statistical copolymerization of HPMA with GlyMA at 50 °C. This is not unexpected given the prior studies reported by Ratcliffe *et al.*[69] and Hatton and co-workers.[70] Thus

essentially all of the desired epoxide functionality within the core-forming block is preserved for post-polymerization cross-linking.

The proportion of GlyMA (15 mol %) selected for statistical copolymerization to produce the core-forming block was informed by observations made by Lovett *et al.*[64] Thus, cross-linked $PGMA_{56}$-P($HPMA_{137}$-*stat*-$GlyMA_7$) worms containing only 5 mol % GlyMA were demonstrated to be unstable with respect to a surfactant challenge. On the other hand, cross-linked $PGMA_{56}$-P($HPMA_{115}$-*stat*-$GlyMA_{29}$) worms containing 20 mol % GlyMA, proved to be stable in the presence of anionic surfactant.[55] However, this relatively high GlyMA content within the core-forming block led to non-thermoresponsive worms. In the present work, it is essential that the nano-objects are sufficiently cross-linked to enable their survival under the high shear homogenization conditions required for the preparation of Pickering emulsions. However, their GlyMA content should not be so high as to prevent a morphological transition occurring on cooling, because such thermoresponsive behavior is required to adjust the mean worm aspect ratio. Given these conflicting requirements, 15 mol % GlyMA was selected to ensure sufficient covalent stabilization, while retaining the desired thermoresponsive behavior.

The $PGMA_{48}$-P($HPMA_{90}$-*stat*-$GlyMA_{15}$) worms prepared at 50 °C formed a soft free-standing gel on cooling to 20 °C, most likely as a result of multiple inter-worm contacts. When the statistical copolymerization of HPMA and GlyMA was complete, this worm gel was immediately diluted from 15% w/w to 7.5 % w/w solids to enable efficient stirring of the shear-thinning gel during the subsequent cross-linking reaction.

The cross-linking protocol utilized in this current study was the same as that reported by Lovett *et al.*[64] The diluted worm gel was spilt into three batches. APTES cross-linker was added (APTES/GlyMA molar ratio = 1.0) to one batch of worms and the resulting aqueous dispersion was stirred overnight at 20 °C to afford relatively long cross-linked worms. A second batch was stored at 4 °C for 2 h to induce a significant reduction in the mean worm aspect ratio,[71] before an equimolar amount of APTES relative to GlyMA

residues was added to obtain relatively short cross-linked worms at 4 °C, see Figure 1. Addition of APTES raised the aqueous solution pH to pH 10, which is required for the initial epoxy-amine step in the cross-linking process.[64] The third batch comprising linear worms was stored at room temperature for various control experiments.

Lovett and co-workers[64] monitored the extent of APTES cross-linking of similar $PGMA_{56}$-P($HPMA_{115}$-*stat*-$GlyMA_{29}$) worms using ^{1}H NMR spectroscopy: the integrated epoxy signal at 3.0 ppm was reduced to 6% of its original value within 8 h at 20 °C. In view of this prior kinetic data, APTES cross-linking for the worms described herein was allowed to proceed overnight at 20 °C. In contrast, APTES was reacted with the short worms formed on cooling for seven days at 4 °C, with this low temperature being maintained to prevent unwanted reformation of the original relatively long worms during covalent stabilization. The resulting long and short cross-linked worms were then characterized by SAXS, DLS, TEM and aqueous electrophoresis.

According to Lovett *et al*.,[64] the APTES cross-linker reacts with the pendent epoxide groups on the GlyMA residues. The three siloxane groups on the former reagent are hydrolyzed *in situ* to form silanols, with multiple condensation reactions producing highly cross-linked worm cores. This covalent stabilization mechanism most likely involves reaction of APTES silanol groups with HPMA residues located on neighboring copolymer chain(s), as well as self-condensation with other partially-reacted APTES species. Moreover, the secondary amines initially formed *via* ring-opening of the epoxide groups can in principle react with a second epoxide, which may also contribute to the overall cross-linking reaction (see Figure S4). Interestingly, studies of the cross-linking kinetics using ^{1}H NMR spectroscopy suggest that the epoxy-amine reaction and the siloxane hydrolysis-condensation reactions occur more or less simultaneously, rather than consecutively.

Dilute aqueous dispersions (0.1% w/w) of the cross-linked long and short worms were subjected to DLS studies and TEM analysis. The former technique reported a sphere-equivalent hydrodynamic diameter of

174 nm for the long worms with a corresponding polydispersity index (PDI) of (0.30). This is somewhat greater than the corresponding diameter obtained for the precursor linear worms (152 nm; PDI = 0.36. This is because cross-linking leads to relatively stiff worms, which have a significantly greater mean persistence length than the highly flexible precursor linear worms. In contrast, DLS studies conducted on the short cross-linked worms indicated an apparent sphere-equivalent hydrodynamic diameter of 55 nm (PDI = 0.19). Furthermore, rheological studies conducted on 0.25% w/w aqueous dispersions of the long and short worms respectively indicated essentially no difference in their solution viscosity (data not shown). Thus the latter parameter can be excluded as a possible explanation for any differences in their Pickering emulsifier performance.

Representative SAXS patterns recorded for both long and short 1.0% w/w $PGMA_{48}$-P($HPMA_{90}$-*stat*-$GlyMA_{15}$) cross-linked worms are shown in Figure 2a. Fitting these SAXS patterns using a previously reported worm micelle model[72] (see Supporting Information) allows the mean aspect ratio of these anisotropic nanoparticles to be determined. From initial trial data fits, it was clear that the persistence length of the short worms should be fixed to their contour length. Table S1 summarizes the overall cross-sectional radius, $R_{sw,}$ of these 'hairy' worms and the worm contour length, L_w, derived from such data fits. According to this analysis, the mean aspect ratios calculated for the long and short worms are 38 and 5.2, respectively. These SAXS data are consistent with the significant difference in worm lengths observed by TEM for these two types of worms (see Figures 2b-2e). *Clearly, substantial variation in nanoparticle anisotropy can be achieved by adjusting the precise reaction conditions used for covalent stabilization of the linear precursor worms.* Moreover, the short worms have similar aspect ratios to the ellipsoidal latexes reported by Vermant and co-workers.[44, 51] Thus a direct comparison of these relatively long and short cross-linked worms as putative Pickering emulsifiers enables the following question to be addressed: does the additional increase in the particle anisotropy lead to enhanced emulsifier performance beyond that already reported for ellipsoidal particles?

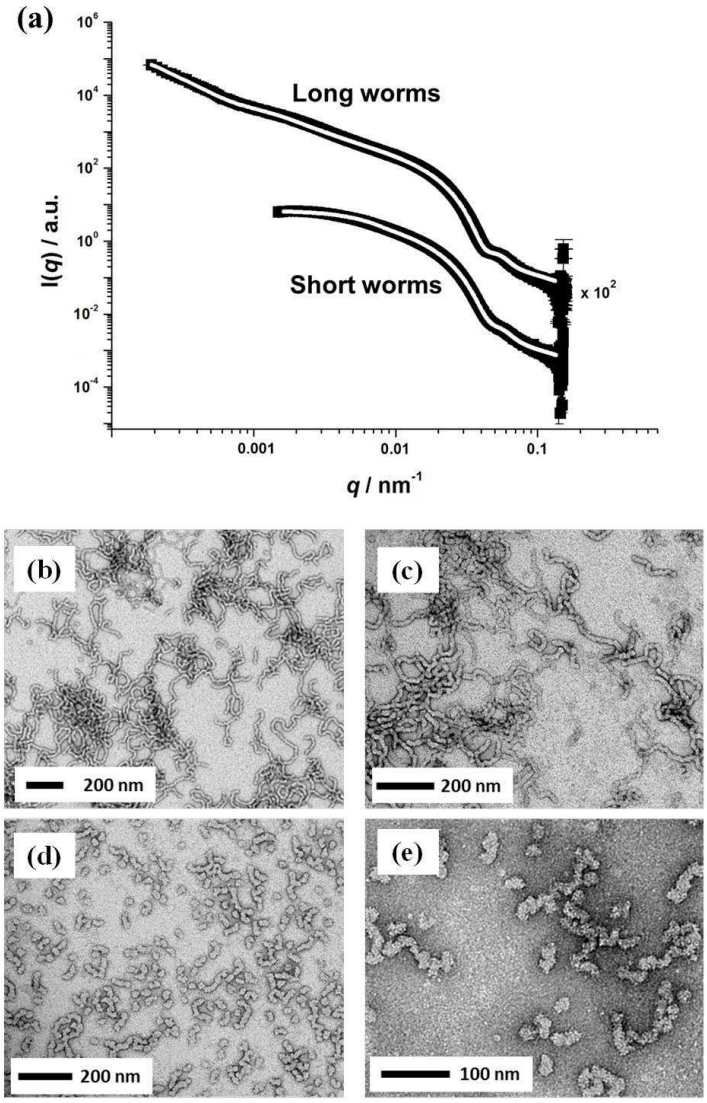

Figure 2. Representative SAXS patterns (black data) and corresponding data fits (white lines) using an established worm micelle model[72] for a 1.0% w/w aqueous dispersion of (a) relatively long $PGMA_{48}$-P($HPMA_{90}$-*stat*-$PGlyMA_{15}$) worms cross-linked at 20°C (mean aspect ratio = 38) and (b) relatively short $PGMA_{48}$-P($HPMA_{90}$-*stat*-$PGlyMA_{15}$) worms cross-linked at 4°C (mean aspect ratio = 5.2). Representative TEM images obtained for long $PGMA_{48}$-P($HPMA_{90}$-*stat*-$GlyMA_{15}$) cross-linked worms prepared at 20 °C after drying (b) a 0.1% w/w aqueous dispersion and (c) a 0.1% w/w methanolic dispersion. Representative TEM images obtained for short $PGMA_{48}$-P($HPMA_{90}$-*stat*-$GlyMA_{15}$) cross-linked worms prepared at 4 °C after drying (d) a 0.1% w/w aqueous dispersion and (e) a 0.1% w/w methanolic dispersion.

In principle, covalent stabilization using APTES should prevent molecular dissolution of these nano-objects in methanol, which is a good solvent for both blocks. Table 1 summarizes the DLS studies conducted on 0.1% w/w dispersions. A modest increase in sphere-equivalent hydrodynamic diameter is observed on transferring the long or short worms cross-linked worms from water to methanol (from 174

nm to 177 nm for the former nanoparticles, and from 55 nm to 63 nm for the latter). Furthermore, the scattered light intensity (derived count rate) remained high in each case. These observations indicate that the cross-linking protocol was successful in both cases: these nano-objects merely become slightly swollen in methanol, rather than undergoing molecular dissolution. Indeed, TEM images confirmed that the original copolymer morphology was preserved on drying dilute copolymer dispersions from methanol (see Figures 2c and 2e). In contrast, the linear $PGMA_{48}$-P($HPMA_{90}$-*stat*-$GlyMA_{15}$) worms exhibit a dramatic reduction in hydrodynamic diameter from 152 nm in water to 51 nm in methanol, which is accompanied by a corresponding substantial reduction in the derived count rate. This indicates that these linear nanoparticles dissociate under such conditions to form molecularly-dissolved copolymer chains.

Table 1. Summary of Dynamic Light Scattering (DLS) Data Obtained for Linear $PGMA_{48}$-P($HPMA_{90}$-*stat*-$GlyMA_{15}$) Worms, Long $PGMA_{48}$-P($HPMA_{90}$-*stat*-$GlyMA_{15}$) Cross-linked Worms and Short $PGMA_{48}$-P($HPMA_{90}$-*stat*-$GlyMA_{15}$) Cross-linked Worms Dispersed in Pure Water, Methanol, and in a 1.0% w/w Aqueous Tween 80 Surfactant Solution.

	water		methanol		1% w/w Tween 80 surfactant	
nanoparticle type	apparent DLS diameter /nm (PDI)	derived count rate /kcps	apparent DLS diameter /nm (PDI)	derived count rate /kcps	apparent DLS diameter /nm (PDI)	derived count rate /kcps
precursor linear worms	152 (0.36)	35 400	51 (0.22)	180	60 (0.18)	26 000
long cross-linked worms	174 (0.30)	56 100	177 (0.27)	41 200	175 (0.29)	42 500
short cross-linked worms	55 (0.19)	26 200	63 (0.14)	17 000	67 (0.20)	32 900

A non-ionic surfactant (Tween 80) was selected to further assess the structural integrity of the cross-linked worms. The same amphiphile was also employed for surfactant challenge experiments on Pickering emulsions (see later). For the precursor linear $PGMA_{48}$-P($HPMA_{90}$-*stat*-$GlyMA_{15}$) worms, the addition of 1.0% w/w Tween 80 led to a substantial reduction in their sphere-equivalent hydrodynamic diameter from 152 nm to 60 nm, with a concomitant significant reduction in the derived count rate. These observations are consistent with those expected for a transition from long worms to short worms.[61] In striking contrast, the long cross-linked worms remained intact when subjected to the same surfactant challenge: no significant change in hydrodynamic diameter or derived count rate was observed by DLS

under such conditions. Similarly, the short cross-linked worms exhibited little change relative to their original dimensions.

Reaction of APTES with the pendent epoxy groups on the GlyMA residues leads to secondary amine formation.[64] Thus the resulting cross-linked nano-objects were expected to acquire weakly cationic character at low pH as a result of protonation of these secondary amine groups. In a control experiment, aqueous electrophoresis studies conducted on a 0.1% w/w aqueous dispersion of precursor $PGMA_{48}$-P($HPMA_{90}$-*stat*-$GlyMA_{15}$) linear worms (i.e. containing no secondary amine functionality) indicated essentially neutral character from pH 3 to pH 10 (see Figure 3).

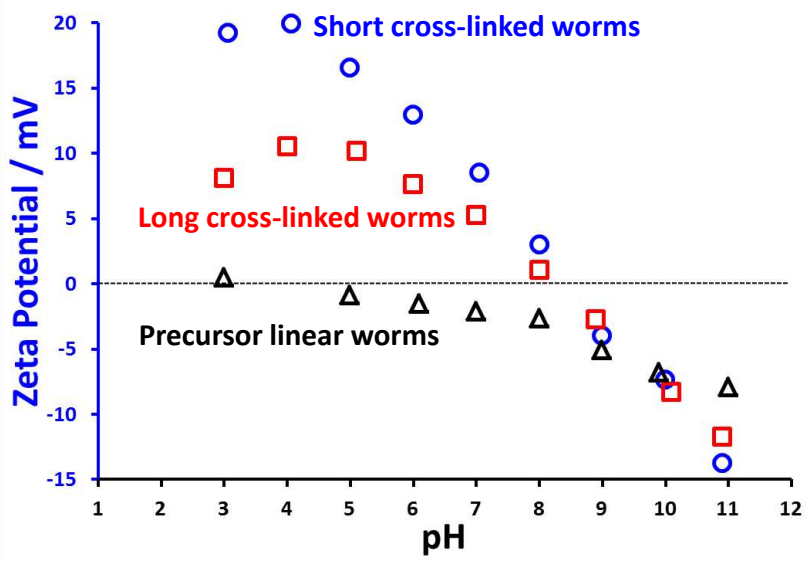

Figure 3. Zeta potential vs. pH curves obtained at 25 °C in the presence of 1 mM KCl for 0.1 w/w aqueous dispersions of precursor linear $PGMA_{48}$-P($HPMA_{90}$-*stat*-$GlyMA_{15}$) worms (black triangles), long $PGMA_{48}$-P($HPMA_{90}$-*stat*-$GlyMA_{15}$) cross-linked worms (blue squares) and short $PGMA_{48}$-P($HPMA_{90}$-*stat*-$GlyMA_{15}$) cross-linked worms (red circles).

In contrast, cross-linked nano-objects exhibited weakly cationic character below pH 8 (see Figure 3). The short cross-linked worms appear to possess appreciably greater cationic character (+19 mV) than the long cross-linked worms (+8 mV) at pH 4. The modest reduction in zeta potential observed at pH 3 is most likely owing to excess HCl acting as a salt, hence screening the cationic surface charge. In principle, both sets of worms should possess comparable cationic character at low pH because they have essentially the same copolymer composition. Of course, the higher zeta potential observed for the short worms at pH 4

may simply indicate that a higher degree of epoxy-amine reaction is achieved at 4 °C for seven days compared to that at 20 °C for approximately 16 h. However, it is emphasized that the electrophoretic data obtained for these anisotropic worms has not been corrected for their non-spherical morphology, as recommended by Ohshima.[73] Moreover, Jones and co-workers reported that $PDMA_{31}$-$PBzMA_x$ spheres, worms and vesicles exhibited differing isoelectric points and cationic character at low pH, despite all three types of nano-objects being prepared using the same poly(tertiary amine methacrylate) steric stabilizer block.[74] Nevertheless, the zeta potentials determined in the present study are consistent with those reported by Lovett *et al*.[64] The weakly anionic character observed at pH 10 (i.e. zeta potentials of -8.2 and -7.2 mV for the long and short cross-linked worms, respectively) may indicate the presence of carboxylic acid end-groups on some of the PGMA stabilizer chains originating from the ACVA initiator used for their RAFT synthesis. Alternatively, this anionic character may simply result from hydroxide ions adsorbing onto the nanoparticle surface at high pH.[75] In this context, it is perhaps noteworthy that the zeta potential of the *linear* worms (-6.8 mV) is comparable to that of both types of cross-linked worms at pH 10.

Evaluation of $PGMA_{48}$-P($HPMA_{90}$-*stat*-$GlyMA_{15}$) cross-linked worms as Pickering emulsifiers. Long and short cross-linked worms were evaluated as putative Pickering emulsifiers for the stabilization of *n*-dodecane droplets in water. In principle, covalent stabilization of these nano-objects should be sufficient to enable them to withstand the high-shear homogenization conditions.[57] A series of aqueous worm dispersions at pH 8 were homogenized with an equal volume of *n*-dodecane at 13 500 rpm for 2 min at 20 °C to produce Pickering emulsions, as depicted in Figure 4.

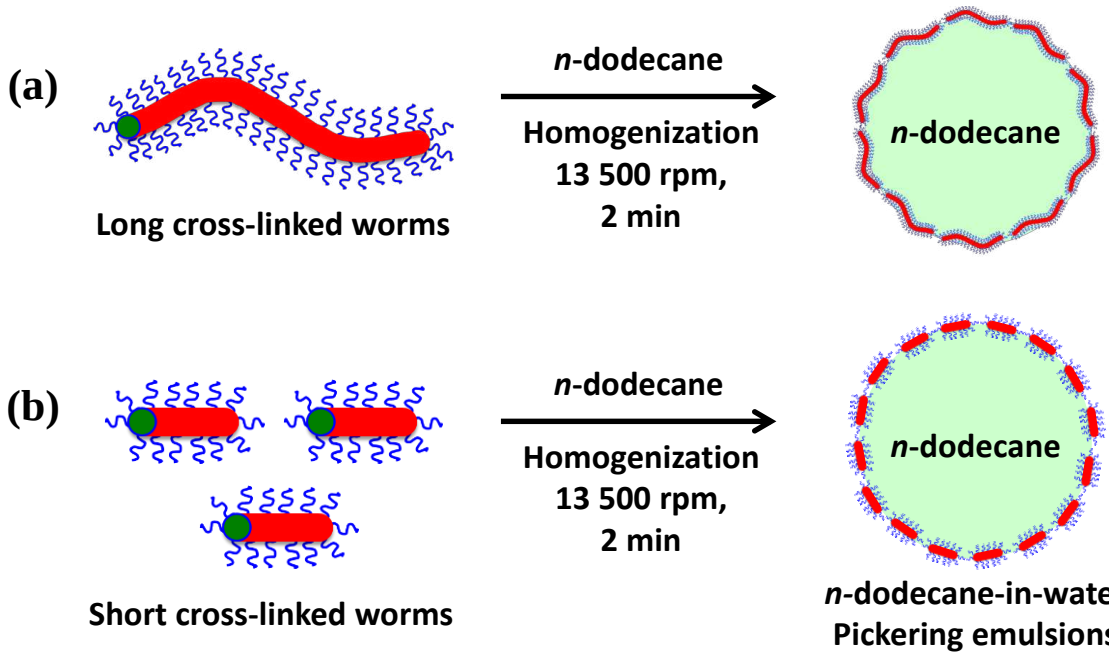

Figure 4. Synthetic route to Pickering emulsions prepared using either (a) long PGMA$_{48}$-P(HPMA$_{90}$-*stat*-GlyMA$_{15}$) cross-linked worms or (b) short PGMA$_{48}$-P(HPMA$_{90}$-*stat*-GlyMA$_{15}$) cross-linked worms. In each case, these worms were cross-linked using APTES, albeit under differing reaction conditions (see main text for further details).

Laser diffraction was used to examine the effect of varying the aqueous copolymer concentration from 0.06 to 2.0% w/w on the mean Pickering emulsion droplet diameter. In a control experiment, varying the concentration of the *linear* PGMA$_{48}$-P(HPMA$_{90}$-*stat*-GlyMA$_{15}$) worms led to a mean droplet diameter of approximately 40 μm in all cases (see Figure 5). Such behavior is typically observed for *soluble* copolymer emulsifiers, indicating that such nanoparticles undergo dissociation during high-shear homogenization to form surface-active copolymer chains.[57] In contrast, systematically increasing the concentration of the *cross-linked* long worms or short worms led to a gradual reduction in the mean droplet diameter until a limiting value was attained (see Figure 5a). This is consistent with the formation of genuine Pickering emulsions.[9, 57, 76] Thus, covalent stabilization of the PGMA$_{48}$-P(HPMA$_{90}$-*stat*-GlyMA$_{15}$) worms is essential to enable them to adsorb intact at the oil/water interface. At lower copolymer concentrations, larger oil droplets are formed because there are fewer nanoparticles available to adsorb at the oil/water interface. In general, the longer worms appear to stabilize slightly finer oil

droplets than the short worms when employed at the same copolymer concentration. However, this effect is relatively weak and is likely to be within experimental error.

Moreover, TEM studies of the dried emulsion droplets (see Figure 5b) confirmed that both the long and short cross-linked worms remained intact after high-shear homogenization. More specifically, densely-packed layers of nanoparticles are observed after evaporation of the oil and aqueous phases under the ultrahigh vacuum conditions required for TEM studies, which provides compelling evidence for the formation of genuine Pickering emulsions. For oil droplets stabilized using long worms, some of these nanoparticles appear to protrude from the edge of the emulsion droplet. Similar observations have been reported for oil-in-water Pickering emulsions stabilized using cross-linked $PGMA_{45}$-$PHPMA_{100}$-$PEGDMA_{10}$ worms.[57] However, this may well be a drying artifact, because evaporation of the internal oil phase causes a gradual reduction in droplet volume. This increases the lateral forces acting on the adsorbed worms and hence might cause some of them to change their orientation relative to the interface.

In principle, the electrophoretic differences indicated in Figure 3 could influence the interfacial activity of the nanoparticles. To investigate this hypothesis, aqueous dispersions of cross-linked nano-objects were adjusted in turn to pH 2, pH 8 or pH 11 prior to homogenization with *n*-dodecane. Overall, the variation in mean droplet diameter under such conditions is rather small for both the long and the short worms (see Figure S5). Thus, protonation of APTES-derived secondary amine groups within the nanoparticle cores appears to have minimal effect on their Pickering emulsifier performance.

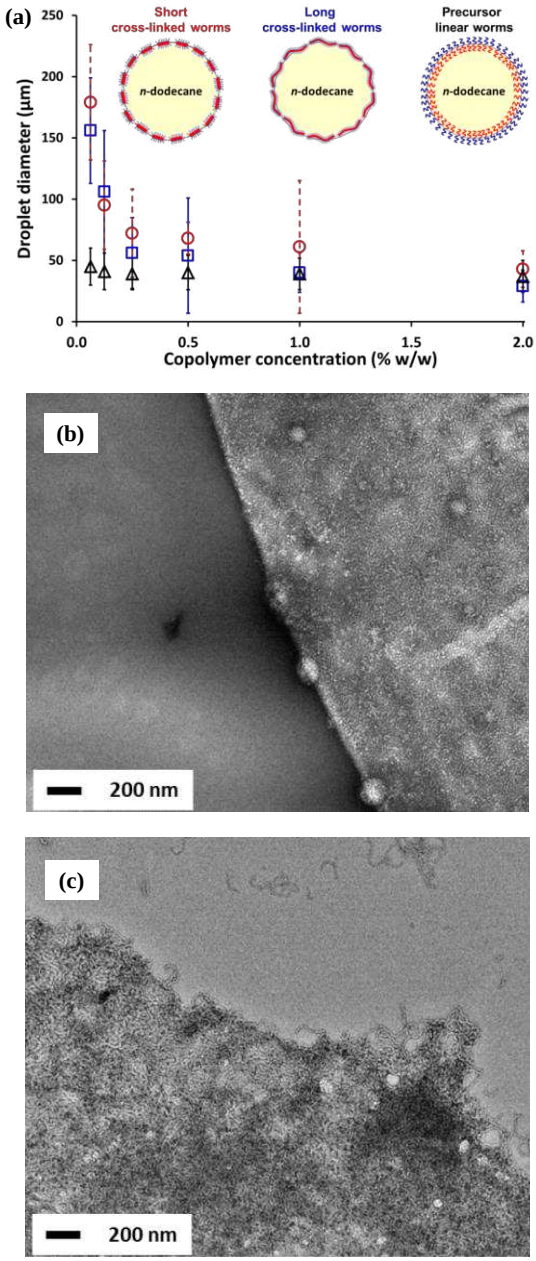

Figure 5. (a) Mean Pickering emulsion droplet diameter (obtained by laser diffraction) *vs*. copolymer concentration plots obtained for the high-shear homogenization of aqueous dispersions of (blue squares) long, (red circles) short PGMA$_{48}$-P(HPMA$_{90}$-*stat*-GlyMA$_{15}$) cross-linked worms or (black triangles) PGMA$_{48}$-P(HPMA$_{90}$-*stat*-GlyMA$_{15}$ precursor linear worms with an equal volume of *n*-dodecane at pH 8. Emulsification conditions: 13500 rpm for 2 min at 20 °C. TEM images of dried Pickering emulsion droplets prepared using (b) 0.06% w/w short PGMA$_{48}$-P(HPMA$_{90}$-*stat*-GlyMA$_{15}$) cross-linked worms and (c) 0.06% w/w long PGMA$_{48}$-P(HPMA$_{90}$-*stat*-GlyMA$_{15}$) cross-linked worms.

Preparation of Colloidosomes. PGMA-PHPMA-PEGDMA cross-linked worms and spheres have been previously examined by Thompson *et al.* for the preparation of covalently cross-linked colloidosomes.[57] This protocol involved using diisocyanate-capped poly(propylene glycol) (PPG-TDI), which is an oil-soluble polymeric cross-linker that readily reacts with the hydroxyl groups on the PGMA

stabilizer chains (and perhaps also the PHPMA core-forming chains) to convert the precursor Pickering emulsions into colloidosomes. In the current study, the preparation of colloidosomes involved homogenization of a 0.25% w/w aqueous dispersion of either long or short worms at pH 3 with an equal volume of *n*-dodecane containing 20.0 g dm^{-3} PPG-TDI cross-linker at 13500 rpm for 2 min at 0 °C. In contrast, our attempts to prepare the same colloidosomes at 20 °C invariably resulted in macroscopic aggregation.[77, 78] In principle, the more nucleophilic secondary amine groups with the cores of the APTES cross-linked nano-objects should react faster with the PPG-TDI than the hydroxyl groups located on the PGMA steric stabilizer. If this leads to faster inter-colloidosome cross-linking, then this would explain the macroscopic aggregation observed when attempting colloidosome syntheses at 20 °C. Lowering the solution pH from pH 8 to pH 3 should protonate the secondary amine groups, as indicated by the aqueous electrophoresis data. If this is the case, then the protonated amine groups formed at low pH should be unable to react with the PPG-TDI cross-linker. It is worth noting that, conducting the homogenisation at pH 3 *or* 0 °C was insufficient to prevent the formation aggregated emulsions. Indeed, preparing such colloidosomes at pH 3 *and* 0 °C resulted in a milky-white emulsion with no visible aggregation. Thus this optimized protocol was adopted in subsequent experiments.

To evaluate their structural integrity, these colloidosomes were subjected to an alcohol challenge whereby excess ethanol was added to remove the oil phase. Moreover, such colloidosomes were prepared using fluorescently-labeled long or short cross-linked worms, which were synthesized by reacting rhodamine B piperazine with a minor fraction of the epoxy groups on the glycidyl methacrylate residues prior to addition of APTES. Successful PPG-TDI cross-linking should enable the detection of intact colloidosomes via fluorescence microscopy after the alcohol challenge. For control experiments conducted on Pickering emulsions prepared in the absence of any PPG-TDI, no surviving microcapsules could be observed after addition of excess ethanol (see Figure S6). In contrast, well-defined colloidosomes prepared using either long or short worms were observed in the presence of excess ethanol. In each case

inter-worm cross-linking produced a robust shell, which possessed sufficient mechanical integrity to remain intact on removal of the oil phase.

Surfactant challenge. Various concentrations of a non-ionic surfactant, Tween 80, were added to Pickering emulsions prepared using a 0.25% w/w aqueous dispersion of either long or short rhodamine B piperazine-labeled cross-linked worms. The resulting emulsions were then inverted several times to ensure adequate mixing and then visualized immediately (within a few minutes). Fluorescence microscopy studies of the initial Pickering emulsions recorded in the absence of any added surfactant confirmed that each type of cross-linked worms was located at the droplet surface, see Figures 6a and 6b. In addition, Figure 6c shows a fluorescence microscopy image recorded for an emulsion prepared using fluorescently-labeled *linear* worms, which dissociate *in situ* under the high-shear emulsification conditions to produce oil droplets that are stabilized by individual copolymer chains, rather than the original worms.

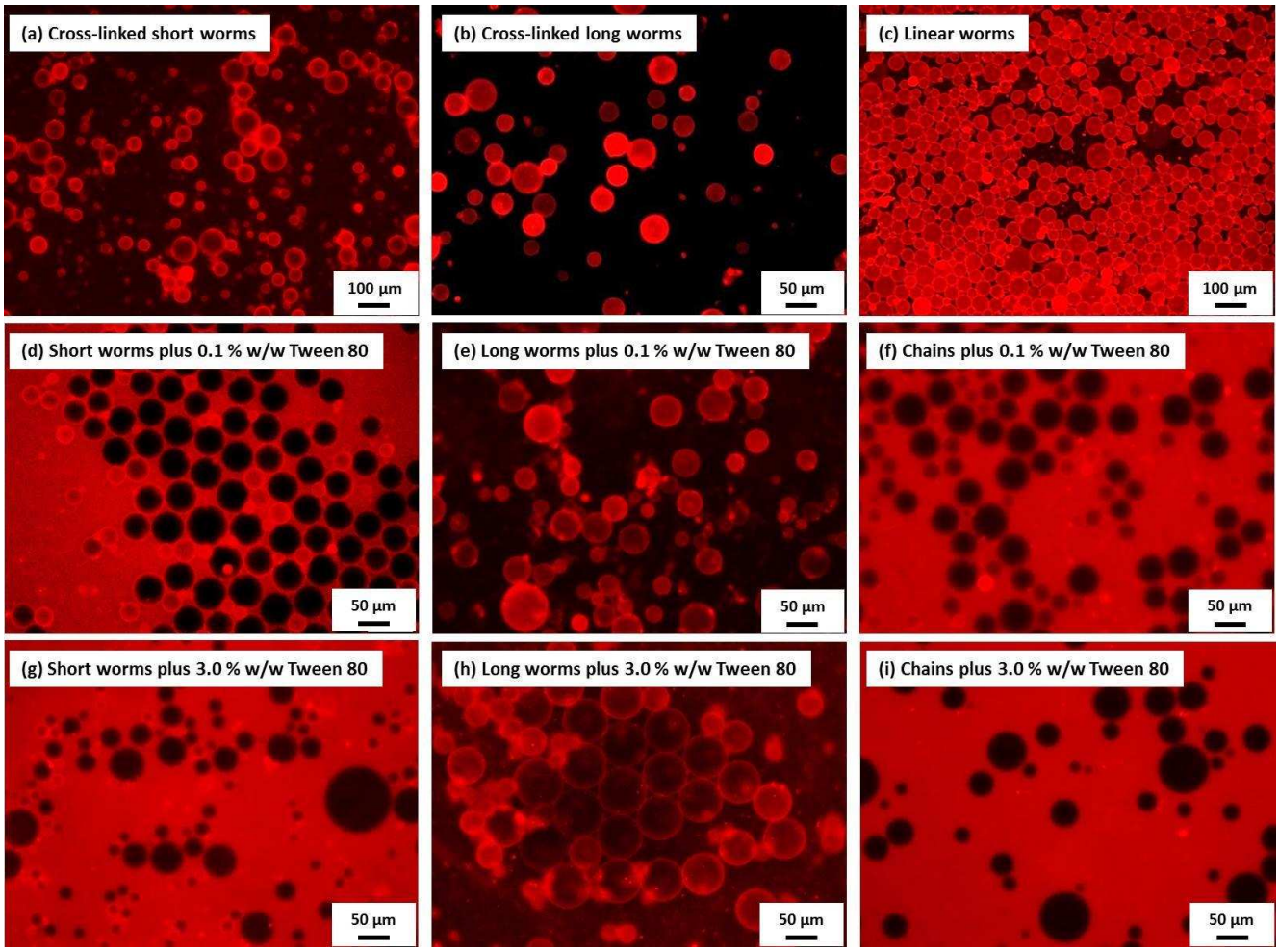

Figure 6. Fluorescence microscopy images obtained for emulsions prepared by high-shear homogenization of 0.25% w/w aqueous $PGMA_{48}$-P($HPMA_{90}$-*stat*-$GlyMA_{15}$) copolymer dispersions with 50 vol % *n*-dodecane at 13500 rpm for 2 min, before and after addition of either 0.1% or 3.0% w/w Tween 80 non-ionic surfactant. (a) Pickering emulsion stabilized by short $PGMA_{48}$-P($HPMA_{90}$-*stat*-$GlyMA_{15}$) cross-linked worms (b) Pickering emulsion stabilized by long $PGMA_{48}$-P($HPMA_{90}$-*stat*-$GlyMA_{15}$) cross-linked worms. (c) Emulsion prepared using precursor $PGMA_{48}$-P($HPMA_{90}$-*stat*-$GlyMA_{15}$) linear worms, which undergo *in situ* dissociation under high shear to produce individual copolymer chains that then act as a polymeric surfactant-type emulsifier (rather than as a genuine Pickering emulsifier). (d) Surfactant-stabilized emulsion obtained after addition of 0.1% w/w Tween 80, which displaces the short worms initially adsorbed at the oil/water interface. (e) Pickering emulsion obtained after addition of 0.1% w/w Tween 80, which does *not* displace the long worms adsorbed at the oil/water interface. (f) Surfactant-stabilized emulsion obtained after addition of 0.1% w/w Tween 80, which displaces the molecularly-dissolved diblock copolymer chains from the oil/water interface. (g) Surfactant-stabilized emulsion obtained after addition of 3.0% w/w Tween 80, which displaces the short worms initially adsorbed at the oil/water interface. (h) Mixed emulsion obtained after addition of 3.0% w/w Tween 80, which *partially* displaces the long worms initially adsorbed at the oil/water interface. (i) Surfactant-stabilized emulsion obtained after addition of 3.0% w/w Tween 80, which displaces the molecularly-dissolved diblock copolymer chains from the oil/water interface.

As shown in Figure 6d, addition of 0.1% w/w Tween 80 to the initial Pickering emulsion results in at least some of the short worms being displaced from the oil/water interface and entering the aqueous continuous phase, as indicated by the highly fluorescent background. Such displacement occurs spontaneously over time scales of the order of a few minutes. Similar results were obtained after addition of 0.1% w/w Tween 80 to the emulsion stabilized by molecularly-dissolved diblock copolymer chains,

see Figure 6e. In contrast, the long worms remained visible at the surface of the oil droplets in the presence of 0.1% w/w Tween 80, see Figure 6f. Even at a surfactant concentration of 3.0% w/w, a significant fraction of the oil droplets remained coated by the worms. However, some background fluorescence is also discernible, indicating that the Tween 80 has displaced at least some of the long worms from the oil/water interface under these conditions. In striking contrast, exposing the emulsions prepared using either the short worms or the molecularly-dissolved copolymer chains to 3.0% w/w Tween 80 clearly results in complete displacement of the original emulsifier from the surface of the droplets, which now appear black owing to their lack of fluorescence. In fact, the copolymer chains could be completely displaced from the oil/water interface at a Tween 80 concentration of just 0.01% w/w (see Figure S7). In summary, these observations serve to highlight the enhanced surfactant resistance exhibited by Pickering emulsions stabilized by relatively long worms compared to that of emulsions prepared using either short worms or molecularly-dissolved copolymer chains *of essentially the same diblock copolymer composition*.

In principle, the surface wettability of the long and short cross-linked worms should be identical. However, the minimum concentration of Tween 80 required to displace the long worms from the interface is around thirty times greater than that required for short worms. This indicates that the long worms are much more strongly absorbed at the oil/water interface than the short worms. This is not surprising given that the SAXS data indicate that the former worms are at least seven-fold more massive than the latter, which implies a similar enhancement in their enthalpy of adsorption at the oil/water interface. In this context, Binks and Horozov[79] expressed the free energy of detachment, ΔG_{dw}, of a rod-like particle into the aqueous phase in terms of its interfacial tension, γ_{ow}, aspect ratio (a/b) and three-phase contact angle θ, as described below in Equation 1.

$$\Delta G_{dw} = \gamma_{ow}\pi b^2(1-\cos\theta)^2\left[1+\frac{4(\frac{a}{b}-1)(\sin\theta-\theta\cos\theta)}{\pi(1-\cos\theta)^2}\right] \qquad (1)$$

Equation 1 provides a quantitative explanation for the difference in surfactant resistance observed for nanoparticles of varying aspect ratio. In the present study, the highly anisotropic worms are much more strongly adsorbed to the oil/water interface, and therefore require significantly more surfactant for their removal compared to less anisotropic worms. Thus highly anisotropic nanoparticles offer an intrinsic advantage for the formation of robust oil-in-water Pickering emulsions. This finding complements recent work by Thompson *et al.,* who reported that cross-linked $PGMA_{45}$-$PHPMA_{100}$-$PEGDMA_{10}$ worms were considerably more *efficient* emulsifiers than the corresponding $PGMA_{100}$-$PHPMA_{200}$-$PEGDMA_{20}$ spheres.[57]

In contrast to the Pickering emulsions shown in Figure 6, fluorescence microscopy studies of colloidosomes prepared using the short cross-linked worms after exposure to 2.0% w/w Tween 80 indicated no significant displacement of the emulsifier from the surface of the oil droplets (compare Figures 7a and 7b). Similar observations were also made for colloidosomes prepared using the long cross-linked worms. These findings are in good agreement with earlier work by Thompson *et al*., who found that colloidosomes prepared using $PGMA_{50}$-stabilized polystyrene latexes in the presence of PPG-TDI exhibited excellent stability when subjected to a surfactant challenge.[80]

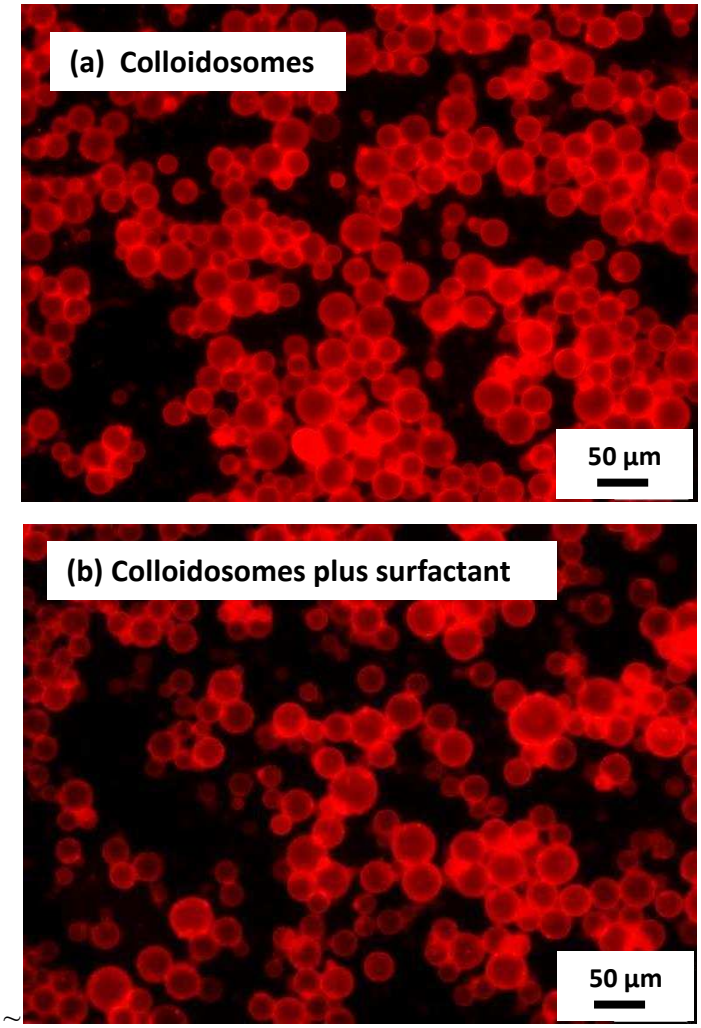

Figure 7. Fluorescence microscopy images recorded for oil droplets prepared via high-shear homogenization of a 0.25% w/w aqueous dispersion of short $PGMA_{48}$-P($HPMA_{90}$-*stat*-$GlyMA_{15}$) cross-linked worms with 50 vol % *n*-dodecane containing 20 g dm^{-3} PPG-TDI. (a) Initial colloidosomes formed after reaction of short cross-linked worms with PPG-TDI at the oil/water interface. (b) Same colloidosomes after addition of 2.0% w/w Tween 80. The lack of difference between these two images confirms that such colloidosomes remain intact in the presence of high levels of non-ionic surfactant.

CONCLUSIONS

Cross-linked worms with markedly differing mean aspect ratios can be prepared via PISA *from the same linear diblock copolymer precursor* using a convenient post-polymerization covalent stabilization protocol. More specifically, linear epoxy-functional $PGMA_{48}$-P($HPMA_{90}$-*stat*-$GlyMA_{15}$) worms were first synthesized by RAFT aqueous dispersion statistical copolymerization of HPMA and GlyMA using a water-soluble PGMA macro-CTA. The epoxy groups in the GlyMA

residues were then ring-opened using APTES in order to cross-link the cores of these relatively long worms at 20 °C. The corresponding relatively short cross-linked worms were prepared by cooling the linear worms to 4 °C so as to reduce their anisotropic character prior to addition of the APTES cross-linker. SAXS studies indicated an approximate seven-fold reduction in the mean aspect ratio for the short worms relative to that of the long worms. DLS and TEM studies of both types of cross-linked worms confirmed that they remained intact on addition of either methanol (a good solvent for both linear blocks) or a non-ionic surfactant (Tween 80). Aqueous electrophoresis studies of these $PGMA_{48}$-P($HPMA_{90}$-*stat*-$GlyMA_{15}$) worms revealed their weakly cationic character below pH 7, which is attributed to protonation of the secondary amine groups within their APTES cross-linked cores. These covalently-stabilized worms were then evaluated as Pickering emulsifiers for the stabilization of *n*-dodecane-in-water emulsions. Unlike the linear precursor worms, both types of cross-linked worms survive high-shear homogenization and hence adsorb as nanoparticles at the oil/water interface to produce genuine Pickering emulsions. The evolution of the mean droplet diameter with homogenization time was investigated in each case. For very short homogenization times, the mean diameter reported by laser diffraction for oil droplets stabilized by short cross-linked worms was significantly greater than that indicated by optical microscopy studies. This suggests that the initial oil droplets were flocculated, most likely via a particle bridging mechanism operating at low surface coverage. However, no such droplet flocculation was observed when using the long cross-linked worms. Robust colloidosomes could also be prepared by adding an oil-soluble polymeric diisocyanate cross-linker, PPG-TDI, to the *n*-dodecane phase prior to high-shear homogenization. However, nanoparticle cross-linking had to be performed under mildly acidic solution (pH 3) at 0 °C in order to avoid the formation of macroscopic aggregates. Pickering emulsions stabilized using either long or short cross-linked worms were exposed to varying concentrations of a non-ionic surfactant

(Tween 80). Fluorescence microscopy studies confirmed that a much higher surfactant concentration was required to displace the long worms from the oil/water interface compared to the short worms. This is because the former nanoparticles are much more strongly adsorbed than the latter. This study provides further evidence for the enhanced Pickering emulsifier performance of highly anisotropic nanoparticles.

ASSOCIATED CONTENT

Supporting Information

^{1}H NMR spectra recorded for the PGMA$_{48}$-P(HPMA$_{90}$-*stat*-GlyMA$_{15}$) statistical diblock copolymer and its PGMA$_{48}$ precursor; DMF GPC traces for the PGMA$_{48}$-P(HPMA$_{90}$-*stat*-GlyMA$_{15}$) statistical diblock copolymer and its PGMA$_{48}$ precursor; effect of varying pH on mean oil droplet diameter for both long and short worm-stabilized Pickering emulsions at various copolymer concentrations; fluorescence micrographs of colloidosomes prepared using either long or short cross-linked worms obtained after an ethanol challenge; fluorescence micrograph of emulsion droplets after adding 0.01% Tween 80 to an emulsion prepared using linear worms.

This material is available free of charge via the Internet at http//:pubs.acs.org.

AUTHOR INFORMATION

Corresponding Authors

*Email k.thompson@manchester.ac.uk (K.L.T.)

*Email s.p.armes@shef.ac.uk (S.P.A)

Present Addresses

†If an author's address is different than the one given in the affiliation line, this information may be included here.

Author Contributions

The manuscript was written through contributions of all authors. All authors have given approval to the final version of the manuscript.

Funding Sources

S.P.A. acknowledges support from EPSRC (EP/J007846/1 and EP/R003009) and is the recipient of a five-year ERC *Advanced Investigator* grant (PISA 320372). Syngenta is thanked for project consumables support and for permission to publish this work.

ACKNOWLEDGMENTS

REFERENCES

1. Pickering, S. U., Emulsions. J. Chem. Soc.Trans. **1907,** 91 (0), 2001-2021.
2. Ramsden, W., Separation of Solids in the Surface-Layers of Solutions and 'Suspensions' (Observations on Surface-Membranes, Bubbles, Emulsions, and Mechanical Coagulation). -- Preliminary Account. Proc. Royal Soc. Lond. **1903,** 72 (477-486), 156-164.
3. Binks, B. P., Particles as surfactants—similarities and differences. Curr. Opin. Colloid Interface Sci. **2002,** 7 (1–2), 21-41.
4. P. Binks, B.; O. Lumsdon, S., Stability of oil-in-water emulsions stabilised by silica particles. Phys. Chem. Chem. Phys. **1999,** 1 (12), 3007-3016.
5. Binks, B. P.; Lumsdon, S. O., Pickering Emulsions Stabilized by Monodisperse Latex Particles: Effects of Particle Size. Langmuir **2001,** 17 (15), 4540-4547.
6. Binks, B. P.; Lumsdon, S. O., Influence of Particle Wettability on the Type and Stability of Surfactant-Free Emulsions. Langmuir **2000,** 16 (23), 8622-8631.
7. Binks, B. P.; Isa, L.; Tyowua, A. T., Direct Measurement of Contact Angles of Silica Particles in Relation to Double Inversion of Pickering Emulsions. Langmuir **2013,** 29 (16), 4923-4927.
8. Ashby, N. P.; Binks, B. P., Pickering emulsions stabilised by Laponite clay particles. Phys. Chem. Chem. Phys. **2000,** 2 (24), 5640-5646.
9. Aveyard, R.; Binks, B. P.; Clint, J. H., Emulsions stabilised solely by colloidal particles. Adv. Colloid Interface Sci **2003,** 100, 503-546.
10. Binks, B. P.; Murakami, R.; Armes, S. P.; Fujii, S., Temperature-Induced Inversion of Nanoparticle-Stabilized Emulsions. Angew. Chem. **2005,** 117 (30), 4873-4876.
11. Saigal, T.; Dong, H.; Matyjaszewski, K.; Tilton, R. D., Pickering Emulsions Stabilized by Nanoparticles with Thermally Responsive Grafted Polymer Brushes. Langmuir **2010,** 26 (19), 15200-15209.
12. Tsuji, S.; Kawaguchi, H., Thermosensitive Pickering Emulsion Stabilized by Poly(N-isopropylacrylamide)-Carrying Particles. Langmuir **2008,** 24 (7), 3300-3305.

13. Zhu, Y.; Fu, T.; Liu, K.; Lin, Q.; Pei, X.; Jiang, J.; Cui, Z.; Binks, B. P., Thermoresponsive Pickering Emulsions Stabilized by Silica Nanoparticles in Combination with Alkyl Polyoxyethylene Ether Nonionic Surfactant. Langmuir **2017,** 33 (23), 5724-5733.
14. Destribats, M.; Lapeyre, V.; Wolfs, M.; Sellier, E.; Leal-Calderon, F.; Ravaine, V.; Schmitt, V., Soft microgels as Pickering emulsion stabilisers: role of particle deformability. Soft Matter **2011,** 7 (17), 7689-7698.
15. Destribats, M.; Lapeyre, V.; Sellier, E.; Leal-Calderon, F.; Ravaine, V.; Schmitt, V., Origin and Control of Adhesion between Emulsion Drops Stabilized by Thermally Sensitive Soft Colloidal Particles. Langmuir **2012,** 28 (8), 3744-3755.
16. Zoppe, J. O.; Venditti, R. A.; Rojas, O. J., Pickering emulsions stabilized by cellulose nanocrystals grafted with thermo-responsive polymer brushes. J. Colloid Interface Sci. **2012,** 369 (1), 202-209.
17. Tu, F.; Lee, D., Shape-Changing and Amphiphilicity-Reversing Janus Particles with pH-Responsive Surfactant Properties. J. Am. Chem. Soc. **2014,** 136 (28), 9999-10006.
18. Fujii, S.; Okada, M.; Furuzono, T., Hydroxyapatite nanoparticles as stimulus-responsive particulate emulsifiers and building block for porous materials. J. Colloid Interface Sci. **2007,** 315 (1), 287-296.
19. Yang, H.; Zhou, T.; Zhang, W., A Strategy for Separating and Recycling Solid Catalysts Based on the pH-Triggered Pickering-Emulsion Inversion. Angew. Chem. Int. Ed. **2013,** 52 (29), 7455-7459.
20. Guo, H.; Yang, D.; Yang, M.; Gao, Y.; Liu, Y.; Li, H., Dual responsive Pickering emulsions stabilized by constructed core crosslinked polymer nanoparticles via reversible covalent bonds. Soft Matter **2016,** 12 (48), 9683-9691.
21. Zhu, Y.; Hu, Q.; Wei, W.; Yi, C.; Liu, X., Core cross-linked and pH-responsive particulate emulsifiers from direct chemical preparation of divinylbenzene with P(AA-r-St) macro-CTA. Colloids Surf. A **2016,** 504, 358-366.
22. Liu, K.; Jiang, J.; Cui, Z.; Binks, B. P., pH-Responsive Pickering Emulsions Stabilized by Silica Nanoparticles in Combination with a Conventional Zwitterionic Surfactant. Langmuir **2017,** 33 (9), 2296-2305.
23. Li, J.; Stöver, H. D. H., Doubly pH-Responsive Pickering Emulsion. Langmuir **2008,** 24 (23), 13237-13240.
24. Haase, M. F.; Grigoriev, D.; Moehwald, H.; Tiersch, B.; Shchukin, D. G., Encapsulation of Amphoteric Substances in a pH-Sensitive Pickering Emulsion. J. Phys. Chem. C **2010,** 114 (41), 17304-17310.
25. Zhao, C.; Tan, J.; Li, W.; Tong, K.; Xu, J.; Sun, D., Ca2+ Ion Responsive Pickering Emulsions Stabilized by PSSMA Nanoaggregates. Langmuir **2013,** 29 (47), 14421-14428.
26. Yang, F.; Liu, S.; Xu, J.; Lan, Q.; Wei, F.; Sun, D., Pickering emulsions stabilized solely by layered double hydroxides particles: The effect of salt on emulsion formation and stability. J. Colloid Interface Sci. **2006,** 302 (1), 159-169.
27. Tan, K. Y.; Gautrot, J. E.; Huck, W. T. S., Formation of Pickering Emulsions Using Ion-Specific Responsive Colloids. Langmuir **2011,** 27 (4), 1251-1259.
28. Bai, R.-X.; Xue, L.-H.; Dou, R.-K.; Meng, S.-X.; Xie, C.-Y.; Zhang, Q.; Guo, T.; Meng, T., Light-Triggered Release from Pickering Emulsions Stabilized by TiO2 Nanoparticles with Tailored Wettability. Langmuir **2016,** 32 (36), 9254-9264.
29. Jiang, J.; Ma, Y.; Cui, Z.; Binks, B. P., Pickering Emulsions Responsive to CO2/N2 and Light Dual Stimuli at Ambient Temperature. Langmuir **2016,** 32 (34), 8668-8675.

30. Chen, Z.; Zhou, L.; Bing, W.; Zhang, Z.; Li, Z.; Ren, J.; Qu, X., Light Controlled Reversible Inversion of Nanophosphor-Stabilized Pickering Emulsions for Biphasic Enantioselective Biocatalysis. J. Am. Chem. Soc. **2014,** 136 (20), 7498-7504.
31. Melle, S.; Lask, M.; Fuller, G. G., Pickering Emulsions with Controllable Stability. Langmuir **2005,** 21 (6), 2158-2162.
32. Zhou, J.; Qiao, X.; Binks, B. P.; Sun, K.; Bai, M.; Li, Y.; Liu, Y., Magnetic Pickering Emulsions Stabilized by Fe3O4 Nanoparticles. Langmuir **2011,** 27 (7), 3308-3316.
33. Yoon, K. Y.; Li, Z.; Neilson, B. M.; Lee, W.; Huh, C.; Bryant, S. L.; Bielawski, C. W.; Johnston, K. P., Effect of Adsorbed Amphiphilic Copolymers on the Interfacial Activity of Superparamagnetic Nanoclusters and the Emulsification of Oil in Water. Macromolecules **2012,** 45 (12), 5157-5166.
34. Katepalli, H.; John, V. T.; Bose, A., The Response of Carbon Black Stabilized Oil-in-Water Emulsions to the Addition of Surfactant Solutions. Langmuir **2013,** 29 (23), 6790-6797.
35. Vashisth, C.; Whitby, C. P.; Fornasiero, D.; Ralston, J., Interfacial displacement of nanoparticles by surfactant molecules in emulsions. J. Colloid Interface Sci. **2010,** 349 (2), 537-543.
36. Alargova, R. G.; Warhadpande, D. S.; Paunov, V. N.; Velev, O. D., Foam Superstabilization by Polymer Microrods. Langmuir **2004,** 20 (24), 10371-10374.
37. Levine, S.; Bowen, B. D.; Partridge, S. J., Stabilization of emulsions by fine particles I. Partitioning of particles between continuous phase and oil/water interface. Colloids Surf. **1989,** 38 (2), 325-343.
38. Chen, T.; Colver, P. J.; Bon, S. A. F., Organic–Inorganic Hybrid Hollow Spheres Prepared from TiO2-Stabilized Pickering Emulsion Polymerization. Adv. Mater. **2007,** 19 (17), 2286-2289.
39. Noble, P. F.; Cayre, O. J.; Alargova, R. G.; Velev, O. D.; Paunov, V. N., Fabrication of "Hairy" Colloidosomes with Shells of Polymeric Microrods. J. Am. Chem. Soc. **2004,** 126 (26), 8092-8093.
40. Kang, D. W.; Park, B. G.; Choi, K. H.; Lim, J. H.; Lee, S. J.; Park, B. J., Geometric Effects of Colloidal Particles on Stochastic Interface Adsorption. Langmuir **2018**.
41. Tu, F.; Park, B. J.; Lee, D., Thermodynamically Stable Emulsions Using Janus Dumbbells as Colloid Surfactants. Langmuir **2013,** 29 (41), 12679-12687.
42. Kim, Y. J.; Liu, Y. D.; Choi, H. J.; Park, S.-J., Facile fabrication of Pickering emulsion polymerized polystyrene/laponite composite nanoparticles and their electrorheology. J. Colloid Interface Sci. **2013,** 394, 108-114.
43. He, J.; Zhang, Q.; Gupta, S.; Emrick, T.; Russell, T. P.; Thiyagarajan, P., Drying Droplets: A Window into the Behavior of Nanorods at Interfaces. Small **2007,** 3 (7), 1214-1217.
44. Madivala, B.; Vandebril, S.; Fransaer, J.; Vermant, J., Exploiting particle shape in solid stabilized emulsions. Soft Matter **2009,** 5 (8), 1717-1727.
45. Anjali, T. G.; Basavaraj, M. G., Shape anisotropic colloids at interfaces. Langmuir **2018**.
46. Guevara, J. S.; Mejia, A. F.; Shuai, M.; Chang, Y.-W.; Mannan, M. S.; Cheng, Z., Stabilization of Pickering foams by high-aspect-ratio nano-sheets. Soft Matter **2013,** 9 (4), 1327-1336.
47. Li, T.; Brandani, G.; Marenduzzo, D.; Clegg, P. S., Colloidal Spherocylinders at an Interface: Flipper Dynamics and Bilayer Formation. Phys. Rev. Lett. **2017,** 119 (1), 018001.
48. Wang, H.; Hobbie, E. K., Amphiphobic Carbon Nanotubes as Macroemulsion Surfactants. Langmuir **2003,** 19, 3091-3093.

49. Briggs, N. M.; Weston, J. S.; Li, B.; Venkataramani, D.; Aichele, C. P.; Harwell, J. H.; Crossley, S. P., Multiwalled Carbon Nanotubes at the Interface of Pickering Emulsions. Langmuir **2015,** 31, 13077-13084.
50. Daware, S. V.; Basavaraj, M. G., Emulsions Stabilized by Silica Rods via Arrested Demixing. Langmuir **2015,** 31, 6649-6654.
51. Madivala, B.; Fransaer, J.; Vermant, J., Self-Assembly and Rheology of Ellipsoidal Particles at Interfaces. Langmuir **2009,** 25 (5), 2718-2728.
52. Kalashnikova, I.; Bizot, H.; Cathala, B.; Capron, I., New Pickering Emulsions Stabilized by Bacterial Cellulose Nanocrystals. Langmuir **2011,** 27 (12), 7471-7479.
53. Svagan, A. J.; Musyanovych, A.; Kappl, M.; Bernhardt, M.; Glasser, G.; Wohnhaas, C.; Berglund, L. A.; Risbo, J.; Landfester, K., Cellulose Nanofiber/Nanocrystal Reinforced Capsules: A Fast and Facile Approach Toward Assembly of Liquid-Core Capsules with High Mechanical Stability. Biomacromolecules **2014,** 15 (5), 1852-1859.
54. Kalashnikova, I.; Bizot, H.; Cathala, B.; Capron, I., Modulation of Cellulose Nanocrystals Amphiphilic Properties to Stabilize Oil/Water Interface. Biomacromolecules **2012,** 13 (1), 267-275.
55. Jiménez Saelices, C.; Capron, I., Design of Pickering Micro- and Nanoemulsions Based on the Structural Characteristics of Nanocelluloses. Biomacromolecules **2018,** 19 (2), 460-469.
56. Kalashnikova, I.; Bizot, H.; Bertoncini, P.; Cathala, B.; Capron, I., Cellulosic nanorods of various aspect ratios for oil in water Pickering emulsions. Soft Matter **2013,** 9 (3), 952-959.
57. Thompson, K. L.; Mable, C. J.; Cockram, A.; Warren, N. J.; Cunningham, V. J.; Jones, E. R.; Verber, R.; Armes, S. P., Are block copolymer worms more effective Pickering emulsifiers than block copolymer spheres? Soft Matter **2014,** 10 (43), 8615-8626.
58. Thompson, K. L.; Fielding, L. A.; Mykhaylyk, O. O.; Lane, J. A.; Derry, M. J.; Armes, S. P., Vermicious thermo-responsive Pickering emulsifiers. Chem. Sci. **2015,** 6 (7), 4207-4214.
59. Fielding, L. A.; Derry, M. J.; Ladmiral, V.; Rosselgong, J.; Rodrigues, A. M.; Ratcliffe, L. P. D.; Sugihara, S.; Armes, S. P., RAFT dispersion polymerization in non-polar solvents: facile production of block copolymer spheres, worms and vesicles in n-alkanes. Chem. Sci. **2013,** 4 (5), 2081-2087.
60. Fielding, L. A.; Lane, J. A.; Derry, M. J.; Mykhaylyk, O. O.; Armes, S. P., Thermo-responsive Diblock Copolymer Worm Gels in Non-polar Solvents. J. Am. Chem. Soc. **2014,** 136 (15), 5790-5798.
61. Blanazs, A.; Verber, R.; Mykhaylyk, O. O.; Ryan, A. J.; Heath, J. Z.; Douglas, C. W. I.; Armes, S. P., Sterilizable Gels from Thermoresponsive Block Copolymer Worms. J. Am. Chem. Soc. **2012,** 134 (23), 9741-9748.
62. Warren, N. J.; Armes, S. P., Polymerization-Induced Self-Assembly of Block Copolymer Nano-objects via RAFT Aqueous Dispersion Polymerization. J. Am. Chem. Soc. **2014,** 136 (29), 10174-10185.
63. Kocik, M. K.; Mykhaylyk, O. O.; Armes, S. P., Aqueous worm gels can be reconstituted from freeze-dried diblock copolymer powder. Soft Matter **2014,** 10 (22), 3984-3992.
64. Lovett, J. R.; Ratcliffe, L. P. D.; Warren, N. J.; Armes, S. P.; Smallridge, M. J.; Cracknell, R. B.; Saunders, B. R., A Robust Cross-Linking Strategy for Block Copolymer Worms Prepared via Polymerization-Induced Self-Assembly. Macromolecules **2016,** 49 (8), 2928-2941.

65. Clarkson, C. G.; Lovett, J. R.; Madsen, J.; Armes, S. P.; Geoghegan, M., Characterization of Diblock Copolymer Order–Order Transitions in Semidilute Aqueous Solution Using Fluorescence Correlation Spectroscopy. Macromol. Rapid Commun. **2015,** 36 (17), 1572-1577.
66. Ilavsky, J.; Jemian, P. R., Irena: tool suite for modeling and analysis of small-angle scattering. J. Appl. Crystallogr. **2009,** 42 (2), 347-353.
67. Li, Y.; Armes, S. P., RAFT Synthesis of Sterically Stabilized Methacrylic Nanolatexes and Vesicles by Aqueous Dispersion Polymerization. Angew. Chem. Int. Ed. **2010,** 49 (24), 4042-4046.
68. Blanazs, A.; Madsen, J.; Battaglia, G.; Ryan, A. J.; Armes, S. P., Mechanistic Insights for Block Copolymer Morphologies: How Do Worms Form Vesicles? J. Am. Chem. Soc. **2011,** 133 (41), 16581-16587.
69. Ratcliffe, L. P. D.; Ryan, A. J.; Armes, S. P., From a Water-Immiscible Monomer to Block Copolymer Nano-Objects via a One-Pot RAFT Aqueous Dispersion Polymerization Formulation. Macromolecules **2013,** 46 (3), 769-777.
70. Hatton, F. L.; Lovett, J. R.; Armes, S. P., Synthesis of well-defined epoxy-functional spherical nanoparticles by RAFT aqueous emulsion polymerization. Polymer Chemistry **2017,** 8 (33), 4856-4868.
71. Inspection of the TEM image shown in Figure 2c confirms that a well-defined spherical morphology was not achieved. Instead, a mixture of spheres, dimers, trimers and a few very short worms were obtained. Similar results were reported by Blanazs et al. (see ref. 52). Nevertheless, this represents a significant reduction in the nanoparticle anisotropy compared to the original worm morphology.
72. Pedersen, J., Form factors of block copolymer micelles with spherical, ellipsoidal and cylindrical cores. J. Appl. Crystallogr. **2000,** 33 (3 Part 1), 637-640.
73. Ohshima, H., Approximate Analytic Expression for the Electrophoretic Mobility of Moderately Charged Cylindrical Colloidal Particles. Langmuir **2015,** 31 (51), 13633-13638.
74. Jones, E. R.; Semsarilar, M.; Blanazs, A.; Armes, S. P., Efficient Synthesis of Amine-Functional Diblock Copolymer Nanoparticles via RAFT Dispersion Polymerization of Benzyl Methacrylate in Alcoholic Media. Macromolecules **2012,** 45 (12), 5091-5098.
75. Marinova, K. G.; Alargova, R. G.; Denkov, N. D.; Velev, O. D.; Petsev, D. N.; Ivanov, I. B.; Borwankar, R. P., Charging of Oil−Water Interfaces Due to Spontaneous Adsorption of Hydroxyl Ions. Langmuir **1996,** 12 (8), 2045-2051.
76. Binks, B. P.; Whitby, C. P., Silica Particle-Stabilized Emulsions of Silicone Oil and Water: Aspects of Emulsification. Langmuir **2004,** 20 (4), 1130-1137.
77. Walsh, A.; Thompson, K. L.; Armes, S. P.; York, D. W., Polyamine-Functional Sterically Stabilized Latexes for Covalently Cross-Linkable Colloidosomes. In Langmuir, American Chemical Society: 2010; Vol. 26, pp 18039-18048.
78. Morse, A. J.; Madsen, J.; Growney, D. J.; Armes, S. P.; Mills, P.; Swart, R., Microgel Colloidosomes Based on pH-Responsive Poly(tert-butylaminoethyl methacrylate) Latexes. Langmuir **2014,** 30 (42), 12509-12519.
79. Binks, B. P.; Horozov, T. S., Colloidal Particles at Liquid Interfaces. Cambridge University Press: Cambridge, 2006.
80. Thompson, K. L.; Armes, S. P., From well-defined macromonomers to sterically-stabilised latexes to covalently cross-linkable colloidosomes: exerting control over multiple length scales. Chem. Comm. **2010,** 46 (29), 5274-5276.